Fracture behaviour of notched as-built EBM parts: characterization and interplay between defects and notch strengthening behaviour

Mirco Peron[a], Jan Torgersen[a], Paolo Ferro[b], Filippo Berto[a]

[a] Department of Industrial and Mechanical Engineering, Norwegian University of Science and Technology, Richard Birkelands vei 2b, 7491 Trondheim, Norway

[b] Department of Engineering and Management, University of Padova, Stradella San Nicola 3, 36100 Vicenza, Italy

Abstract

Additive manufacturing (AM) offers the potential to economically produce customized components with complex geometries. However, the introduction of complex geometry goes hand in hand with the presence of notches. Thus, the basic understanding of the tensile behaviour of AM fabricated notched components must be substantially improved so that the unique features of this rapidly developing technology can be utilized in critical load bearing applications. This work aims to assess the tensile behaviour of different notched specimens manufactured by means of the Electron Beam Melting (EBM) technology and tested in their as-built conditions in order to reveal the interplay between notch geometry and AM specific processing. Scanning Electron Microscopy (SEM) was used to investigate the fracture surface of the broken samples, revealing the presence of process-induced defects, harmfully affecting tensile strength with a reduction of 10% and elongation to failure with 40% with respect to values reported in literature for heat treated AM parts, respectively. Interestingly, the authors have discovered an increase in the tensile strength with the severity of the stress concentrators, quite contrary to what is commonly observed for wrought Ti-6Al-4V. This notch strengthening behaviour particular to AM specimens is related to the influence of defects on the failure driving force. The authors provide a qualitative explanation for this phenomenon using 3D FE analyses together with a theoretical description via the ellipse criterion.

Keywords: EBM; additive manufacturing; notch; defects; voids; notch strengthening; tensile strength.

1. Introduction

Since its introduction almost four decades ago [1], additive manufacturing (AM) has experienced a steady growth through the years taking advantage of its layer-by-layer manufacturing approach that offers unprecedented possibilities in shape complexity and custom geometry [2–5]. The capability to manufacture components with limited manufacturing constraints is especially beneficial in structural applications when combined with methods for structural optimization [6–8]. Owing to the growing importance of AM technologies, researchers have focused on developing fundamental theoretical understanding of mechanical properties of additively manufactured metals, especially Ti-6Al-4V, aiming to obtain AM parts with a mechanical behaviour and a reliability that allows the replacement and redevelopment of conventionally manufactured components. Various research papers deal with the impact of processing conditions on the mechanical properties such as yield and tensile strength. In this regard, Abdeen and Palmer studied the effect of the beam current, beam speed and offset focus on density of Ti-6Al-4V specimens manufactured by means of Electron Beam Melting (EBM) technology. They found the density to be highly influenced by the offset focus: changing the offset focus from 0 to 25 mA resulted in an almost 10 per cent decrease in density due to the increase in porosity [9]. Besides studying the influence of powder layer thickness on the relative density of components obtained by means of Selective Laser Melting (SLM) technology, Sufiiarov et al. investigated the effect of defects on the mechanical properties and the dependence of mechanical properties on the growth direction. Specimens manufactured parallel to the main platform of the Selective Laser Melting (SLM) system are characterized by higher yield and tensile strength [10]. The influence of microstructural flaws on the mechanical properties has also been studied by Gong et al. [11]. In their work, they induced defects in either SLM or EBM Ti-6Al-4V components and assessed their effects on tensile, fatigue and hardness properties. They reported that in Electron Beam Melting (EBM) technology any significant deviation from the optimum process parameters results in relatively large defects and poor mechanical properties. In SLM samples, small pores or voids are harmless when present in amounts up to 1 vol.%. Instead, the mechanical properties are reduced considerably when defects occur at levels of 5 vol.%. Several authors compared the mechanical properties of components

manufactured by means of AM and of conventional processes [12,13] and the tensile strength of SLM and EBM components [14,15]. Despite these significant advances in understanding the impact of processing conditions on the mechanical behaviour of parts, the effect of geometric discontinuities such as notches is so far underexplored. Yet, this is highly relevant in the field of complex geometric design as such attempts naturally introduce such discontinuities reported to strongly affect both tensile and fatigue properties of the components [16-26]. In fatigue, the effect of notches is unambiguous, determining a reduction in the fatigue strength for several materials [27–34]. Concerning tensile strength, instead, notched specimens have been reported to be characterized either by a notch strengthening or by a notch weakening behaviour [35–37]. Ductile materials, such as Ti-6Al-4V and Al T6061, are characterized by a notch strengthening effect [38,39], whereas brittle materials, such as Al_2O_3 and Ti_3SiC_2, by a notch weakening behaviour [39,40]. Aiming to contribute to the fundamental understanding of the effect of notches on EBM parts, tensile tests on un-notched and notched Ti-6Al-4V specimens have been herein carried out. The notch strengthening behaviour for EBM parts herein tested has been found to differ significantly from that reported for their wrought counterparts [38]. In what follows, a qualitative understanding leveraging on 3D FE analyses and on a failure criterion, i.e. the ellipse criterion, has been provided. To reveal the interplay between notch geometry and AM specific processing, EBM specimens have been tested in their as-built conditions.

2. Materials and Method

The material tested is Ti-6Al-4V obtained using the EBM technology manufactured by FIT Prototyping GmbH (Lupburg, Germany) and the process parameters used are listed in Table 1.

Setting	Value
Hatch Line offset	200 µm
Number of contours	4
Power (max, electron gun)	3000 W

Table 1. EBM settings used during the manufacturing of the samples. Data provided by the manufacturer.

Quasi-static tensile tests (ten for each specimen geometry) were carried out on as-built samples by using a universal MTS machine (50 kN). All the tests have been carried out with a crosshead speed of 0.2 mm/min and an axial MTS extensometer MTS632.29F-30 was mounted on all the specimens. In this way, the tensile

behaviour of four different geometries was investigated, i.e. dog-bone, semi-circular notched and two blunt V-notched specimens characterized by different notch root radii. Sample geometries are reported in Figure 3, and they were fabricating stacking layers of material along the loading direction (Z-direction).
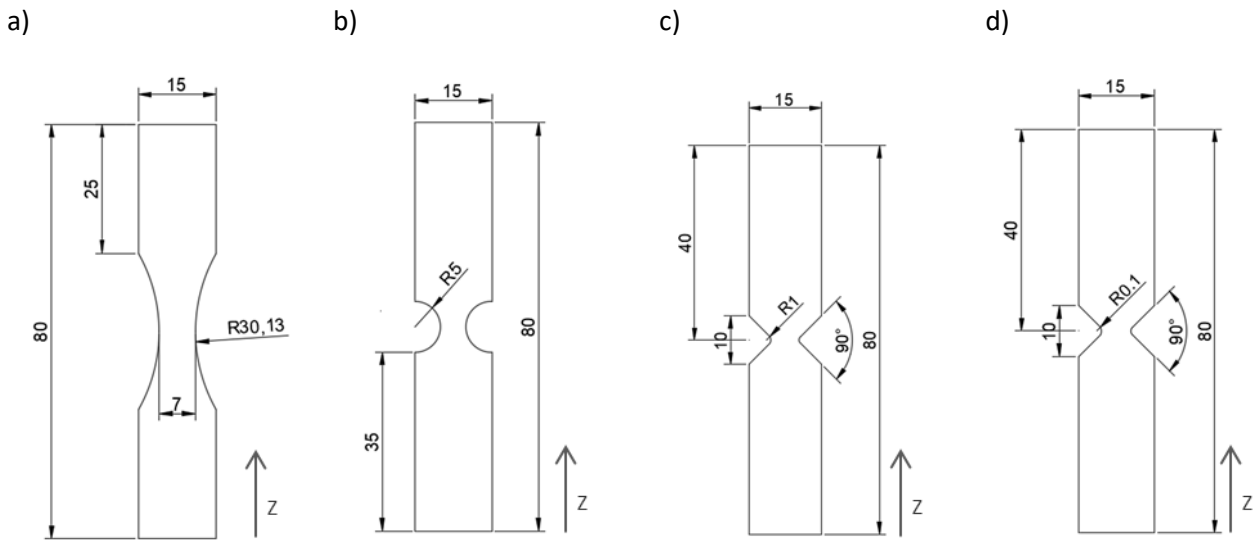
a)   b)   c)   d)

Figure 3. Samples geometries: (a) dog-bone specimen, (b) semi-circular specimen, (c) blunt V-notch specimen with a notch root radius of 1 mm, and (d) blunt V-notch specimen with a notch root radius of 0.1 mm

All the samples were characterized by a thickness of 5 mm and they were not post-processed by either heat or surface treatment. The tensile behaviour of EBM notched specimens in the as-built condition. The fracture surfaces of the samples were investigated by Scanning Electron Microscopy (SEM).

3. Notch strengthening effect

Dealing with tensile behaviour, notches have a dual effect: they strengthen ductile materials, whereas they weaken brittle materials. Since Ti-6Al-4V is a ductile material, only the notch strengthening effect is relevant here. To understand its occurrence, the stress distributions ahead of the notch tip needs to be considered. In the un-notched specimens, the stress-state is uniaxial, and the specimen fails when the principal stress equals the tensile strength of the material, σ_{UTS}, as it can be seen from the Mohr's stress circle in Figure 4.
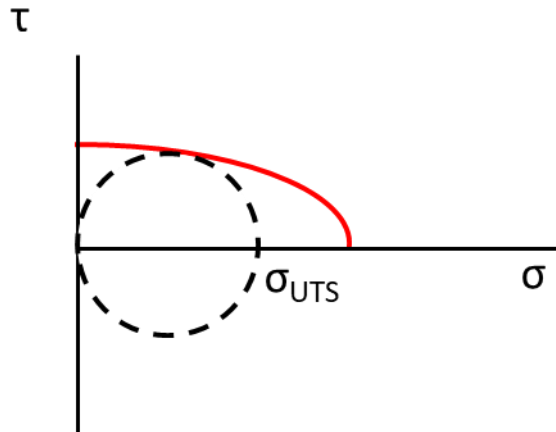
Figure 4. Mohr's circle for un-notched specimens. The red line is defined in Eq. 1

In the notched specimens, the stress state in the proximity of the notch is more complex. The stress state becomes tri-axial, except at the notch tip where for equilibrium condition it is bi-axial. Indeed, when the nominal stress reaches the yield strength, the material in the notched section attempts to stretch plastically in the direction parallel to the loading axis. Due to the conservation of volume during the plastic deformation process, the material around the notch root also tries to contract, but is constrained by the bulk of the sample which is still in an elastic stress state. The increment of tensile stresses in the other two principal directions reduces the local shear stress and influences the Mohr's stress circles, which become smaller, necessitating a raise of the axial stress to initiate plastic deformation and failure (Figure 5).
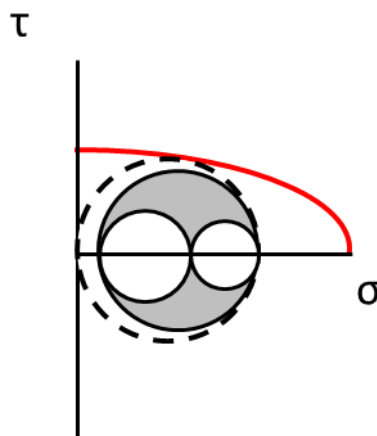
Figure 5. Mohr's circle for notched specimens evaluated at the boundary between the plastic zone and the

elastic zone in ductile materials. Dashed circle represents the Mohr's circle for un-notched components

(Figure 4). The red line is defined in Eq. 1

According to the ellipse criterion proposed by Zhang and Eckert [41], failure occurs when the Mohr's stress

circle intersects the critical failure line defined in Eq. 1 (red line in Figures 5 and 6) at a certain critical point,

i.e. the boundary between the plastic zone and the elastic zone [40].

$$\tau^2 + \alpha^2\sigma^2 = \tau_0^2$$

(1)

In equation (1), τ_0 is the critical shear fracture strength and α is the ratio between τ_0 and the normal

fracture strength (σ_0). For the determination of τ_0 and σ_0, the reader should refer to Ref. [42].

If the Mohr's stress circle becomes smaller, a higher normal stress needs to be applied to reach the failure

condition. According to this criterion, the increment in the tensile strength decreases with increasing the

stress concentration factor K_t [40]. Wrought Ti-6Al-4vV have been previously tested by the authors with

different notch geometries, and the results agree with the statement just reported [38].

4. Results
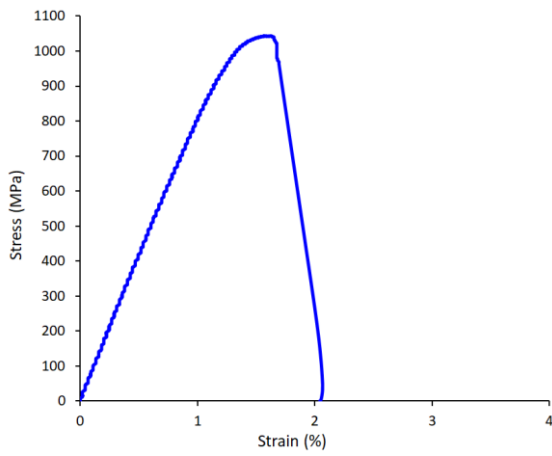
4.1. Tensile test results

For the sake of clarity, just one stress-strain curve for each notch geometry is reported in Figure 6 and the

tensile strengths for each specimen geometry are summarized in Table 2, where bold numbers represent

the average values and numbers in brackets the relative standard deviation.

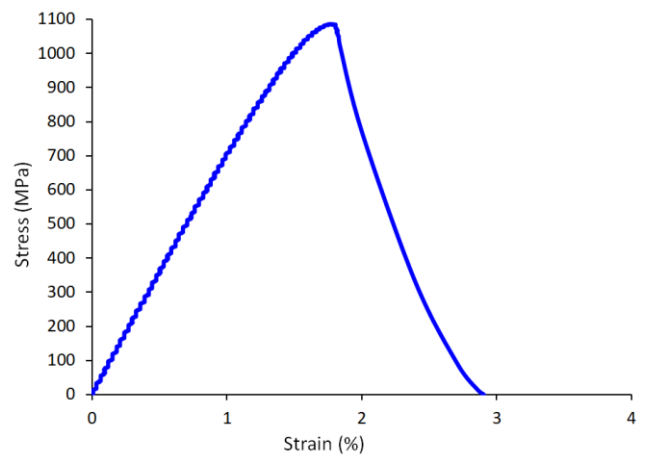a)   b)
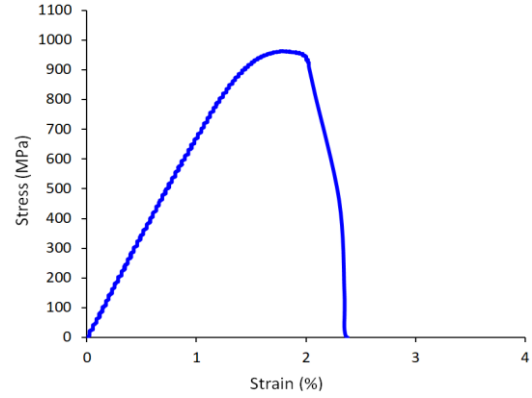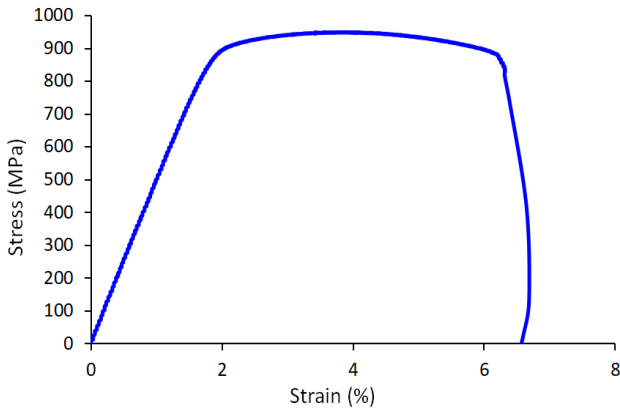
Figure 6. Stress-strain curves for dog-bone (a), semi-circular (b), blunt V-notched AM specimens with a

notch radius of 1 mm (c) and 0.1 mm (d)

Specimen geometry	Tensile strength (MPa)
Dog-bone	**942.86** (8.7)
Semi-circular	**950.4** (23.5)
Blunt V-notch (radius 1 mm)	**1055.16** (10.2)
Blunt V-notch (radius 0.1 mm)	**1080.75** (33.3)

Table 2. Tensile strength for each AM specimen geometries

From the just mentioned results, two main points can be observed, and they will be analysed in detail in

the discussion session:

- the more severe the stress concentrators, the higher the tensile strength, contrary to what observed for wrought Ti-6Al-4V;

- a lower strain to failure and tensile strength have been found compared to the values reported in literature for either surface or heat treated AM samples [12,14].

4.2. Fractography

After each tensile test, the fracture surfaces of each notched specimen have been analysed by means of SEM. Different magnifications have been used to investigate the presence of process-induced defects and characterize the fracture behaviour, i.e. whether brittle or ductile failure has occurred. The results showed a good agreement between fracture surfaces of the different notch geometries, and for the sake of brevity only the fracture surfaces of the dog-bone specimen will be shown. Figure 7 depicts the typical defects observable in EBM additively manufactured components; Figure 7a reports the presence of un-melted particles, whereas Figure 7b shows voids due to incomplete re-melting and lack of fusion, resulting in flat irregular-shaped pores with sharp angles with an average size of 200 µm. These defects have been found mostly inside the material, and closest voids have been measured to be 620 µm, 680 µm and 660 µm from the notch tip for semi-circular, blunt V-notched with a notch root radius of 1 mm and 0.1 mm specimens, respectively (Figure 9).
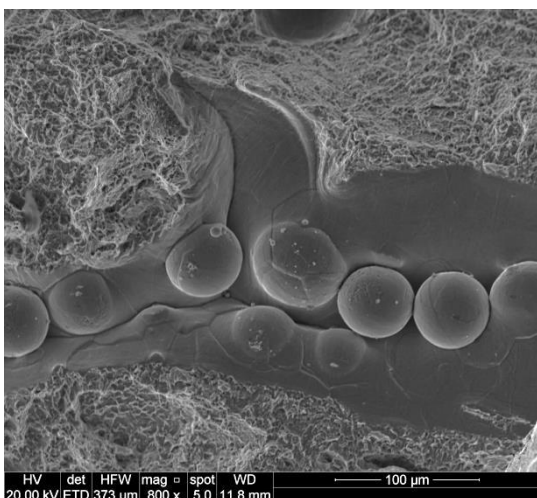
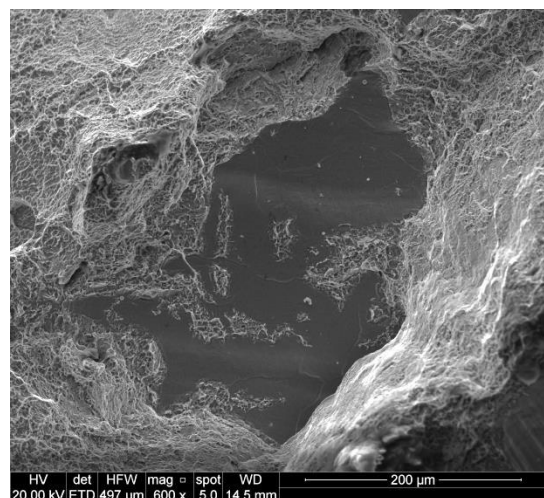a)   b)

Figure 7. Particularity of the process-induced defects: un-melted particles (a) and void formation due to air

entrapment (b)

In addition, the high residual stresses introduced by the manufacturing process induce the formation of

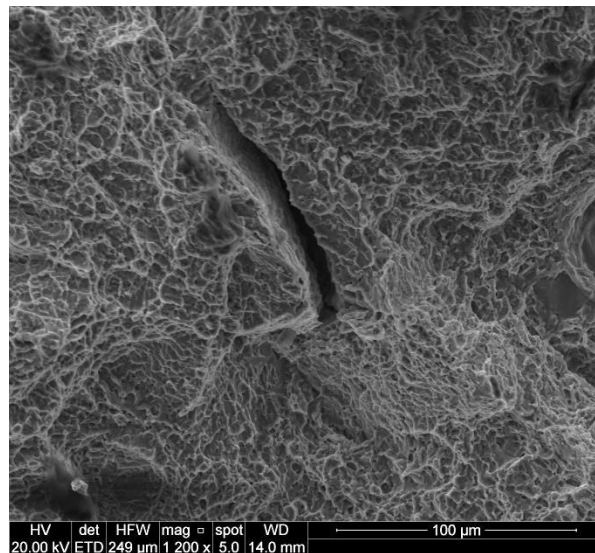cracks within the specimens already after manufacturing (Figure 8).

Figure 8. Detail of a crack induced by the process-induced residual stresses
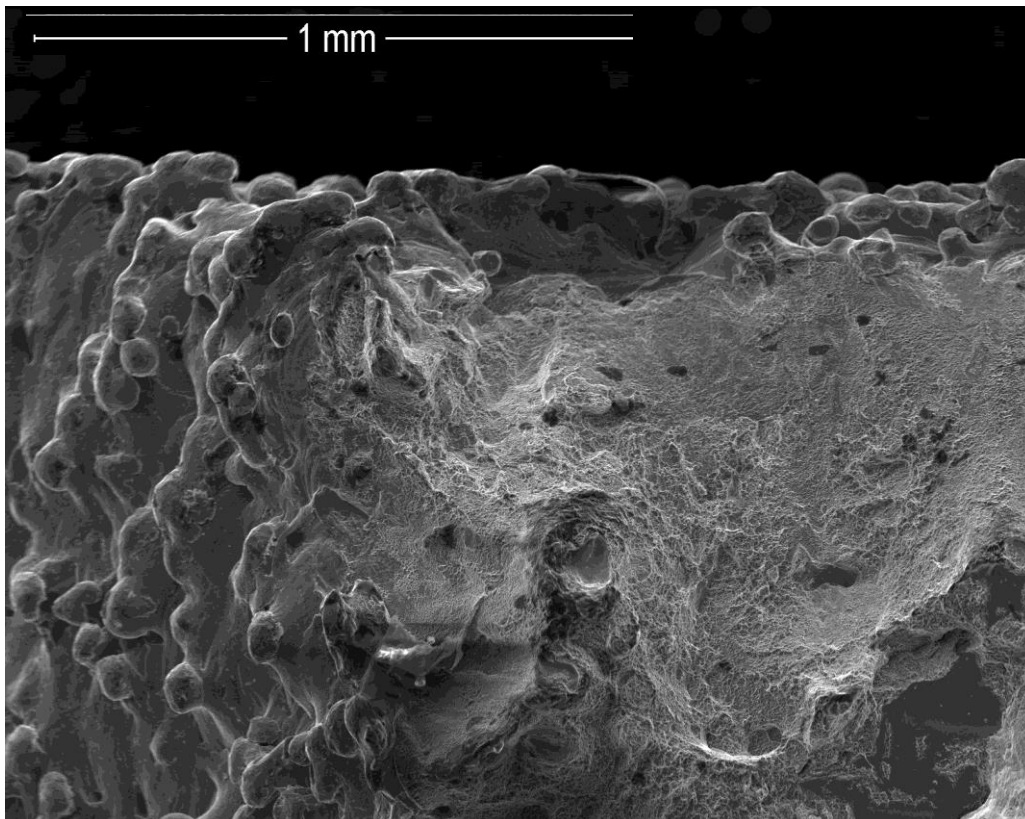
Figure 9. Detail of one of the closest flaw to the specimen surface.

The final fracture surface characterized by dimples (Figure 10) proved a ductile behaviour of as-built EBM parts.
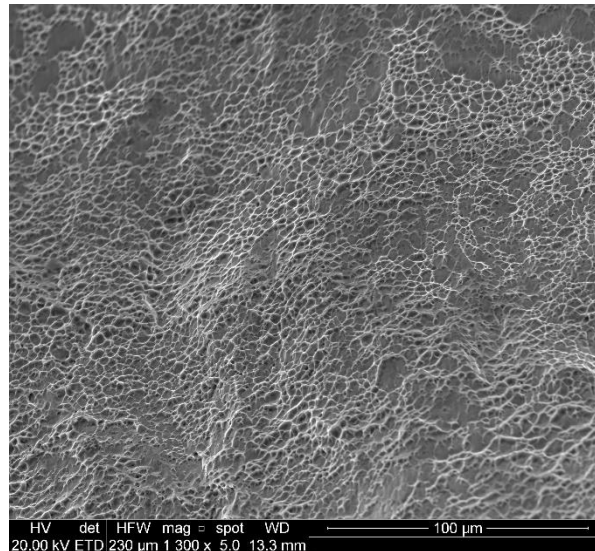

Figure 10. Detail of the dimples characterizing the fracture surfaces of as-built EBM components

5. **Discussion**

In the results section, two main points have been highlighted;

1. The lower mechanical properties (strain to failure and tensile strength) compared to those obtained for either surface or heat treated AM samples.

2. An increase in the tensile strength with the severity of the notch, contrary to what observed for wrought Ti-6Al-4V.

Related to 1, the elongation to fracture of about 6.5% obtained for the as-built dog-bone specimens is far lower than that found by Tong et al. for hot isostatic pressed (HIP) EBM parts (>12%) as well as the tensile strength (943 MPa instead of almost 1000 MPa) [14]. This is due to the presence of defects in the as-built specimens. HIP is in fact a process that, combining heat treatment with externally applied pressure, aims to reduce the amount of porosity in the as-built material. The results herein reported agree with those found by Gong et al. [11]. They investigated the effects of different combinations of process parameters on the

mechanical properties of both SLM and EBM components. They reported how a porosity of 5 vol.% on EBM samples decreases the elongation to fracture of almost 95% and tensile strength from 1012 MPa to 423 MPa.

Related to 2, the tensile strength has been found to increase with the severity of the notch (Table 2). This disagrees with the results obtained by the authors for wrought Ti-6Al-4V [38], where semi-circular specimens were characterized by a higher ultimate tensile strength (UTS) than blunt V-notched specimens with a notch root radius equal to 1 mm, the latter considered to be a much more severe notch. This can be attributed to the presence of voids in the AM components. Fracture is related to the absolute volume of material experiencing high stresses. With notch severity at constant overall dimensions, the volumes of highly stressed material gets smaller and therefore it is statistically less significant that a smaller volume contains strength reducing defect [43].

To substantiate this hypothesis, we aim to provide a qualitative explanation employing the ellipse fracture criterion. According to this model, failure is governed by the three principal stresses distributions at the boundary between the plastic zone and the elastic zone. These stresses have thus been assessed at this critical point, first considering the material homogeneous and then introducing a defect at the experimentally observed closest locations (in section 4.2). The critical point has been evaluated as the location where the Von Mises equivalent stress equals the yield strength of the un-notched material, i.e. at 917 MPa, when the failure load is applied (Table 3).

Specimen geometry	Boundary location (mm)
Semi-circular	0.35
Blunt V-notch (notch tip radius 1 mm)	0.19
Blunt V-notch (notch tip radius 0.1 mm)	0.16

Table 3. Distance from the notch tip of the boundary between the plastic zone and the elastic zone.

The yield strength has been defined as the stress leading to a 0.2% plastic deformation upon load removal. The Von Mises equivalent stress has been evaluated by means of linear elastic 3D finite element (FE) analyses using Ansys®, considering the material to be homogeneous and isotropic. The three principal stresses considering the material is dense and isotropic are reported in Table 4 for the three notched geometries.

Main stress \ Geometry	Semi-circular	Blunt V-notch (notch tip radius 1 mm)	Blunt V-notch (notch tip radius 0.1 mm)
σ_1 (MPa)	1136.4	1922.7	2157.7
σ_2 (MPa)	75.1	375.5	553.3
σ_3 (MPa)	21.7	324.5	487.9

Table 4. Three principal stresses for the three notched geometries considering material homogeneity.

Now, considering the presence of flaws within the material, an idealized spherical defect within the material has been modelled and located at the closest position from the notch surface reported in section 4.2. The radius of the defect (200 µm) corresponds to the average defect radius observed from the analyses of the fracture surfaces. As a proof of concept of this approach, we are modelling one AM void at this point and more details about the finite element models can be found in the Appendix. A more complex scenario replicating AM specific material distribution is subject to future work (manuscript in preparation). The three principal stresses of the specimens containing defects are gathered in Table 5.

Main stress \ Geometry	Semi-circular	Blunt V-notch (notch tip radius 1 mm)	Blunt V-notch (notch tip radius 0.1 mm)
σ_1 (MPa)	1249.6	1974.9	2202.3
σ_2 (MPa)	150.37	387.7	514.6
σ_3 (MPa)	13.9	325.7	491.9

Table 5. Three principal stresses for the three notched geometries considering a single spherical defect within the material.

Being the failure governed by the Mohr's circle defined by the first and third principal stresses according to the ellipse criterion, the introduced defect determines an increase in its radius of 10.9%, 3.2% and 2.4% for semi-circular, blunt (notch root radius 1 mm) and V-notched (notch root radius 0.1 mm), respectively. The influence of flaws on the semi-circular specimens is higher than in blunt V-notched, leading to a reduction of the notch strengthening effect. This is in line with what mentioned above, i.e. that more severe notched components are characterized by lower volumes of highly stressed material, that are therefore less likely containing strength reducing defects.

6. Conclusions

The mechanical properties of as-built EBM parts weakened by different notch geometries have been investigated. The presence of process-induced defects such as voids, cracks and un-melted particles affect the mechanical properties of AM parts, broadly reducing the elongation to failure and the tensile strength by almost 40% and 10%, respectively, with respect to values reported in literature, respectively. Moreover, the presence of notches have been revealed to increase the tensile strength of the as-built EBM parts herein tested, and the tensile strength has been found to increase with the severity of the notch. This disagrees with the results obtained for wrought Ti-6Al-4V, where the increment in the tensile strength decreases with increasing the stress concentration factor. Explanations have been found considering the presence of defects within the material. Utilizing 3D FE analyses together with the ellipse criterion, the failure driving force of the semi-circular specimens has been revealed to highly increased by the presence of defects, contrary to that for the blunt V-notched specimens. These findings can help designers of complex geometries to better predict the failure of their components and potentially identify suitable countermeasures.

Appendix

3D FE analyses have been carried out by means of Ansys®, using 20-nodes solid elements 186. When dealing with flawless models, the material has been considered homogeneous and isotropic, with a Young's modulus of 113.8 GPa and a Poisson's ratio of 0.342. Fine mesh (element size of 10^{-4} mm) has been used in

the proximity of the notch tip to describe accurately the stress distribution (Figure A1). Mesh has then been coarsened getting away from the analysed area. Moreover, considering the symmetry of the geometry, only one quarter has been modelled.
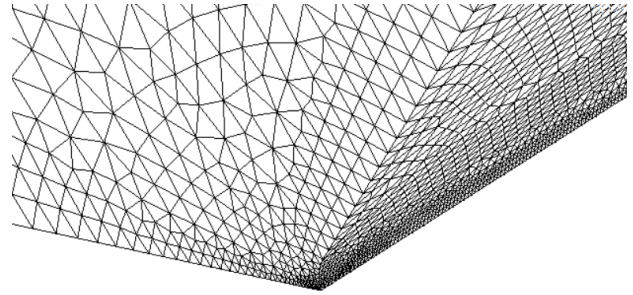
a)
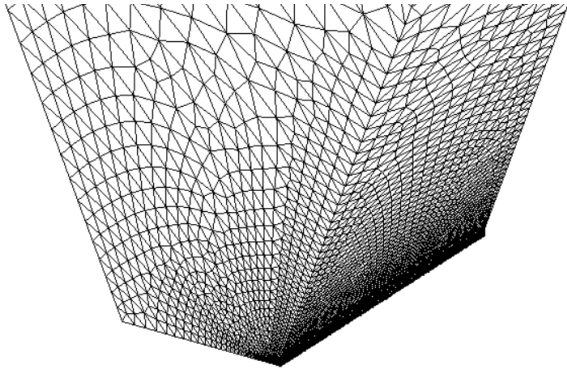
b)

Figure A1. a) Mesh on the flawless blunt V-notched specimen with radius 0.1 mm. b) Detail of the mesh at the notch tip

When modelling defects within the material, a spherical defect with radius 200 μm has been introduced. As mentioned in the text, 200 μm is the average defect radius observed from the analyses of the fracture surfaces. Aiming this work to provide a qualitative explanation of the increasing influence of defects on less severe notched components, only one void has been modelled. Modelling the complex scenario replicating AM specific material distribution is in fact out of the scope of this work and is subject to future work (manuscript in preparation). The defect has been located at the closest position from the notch surface. These locations are reported in section 4.2. and have been obtained from fractographic analyses. Symmetry conditions have been used and the defect has been modelled as a quarter of a sphere (coloured in red in Figure A2).
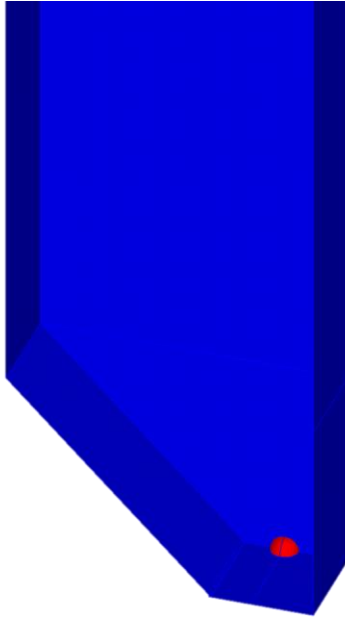
Figure A2. Schematic representation of the blunt V-notched specimen with radius 0.1 mm where the red

quarter of sphere represent the defect within the material

Fine mesh (element size of 10^{-4} mm) has been used at the notch tip area close to the defect and in its

proximity to describe accurately the stress distribution (Figure A3). Mesh has then been coarsened getting
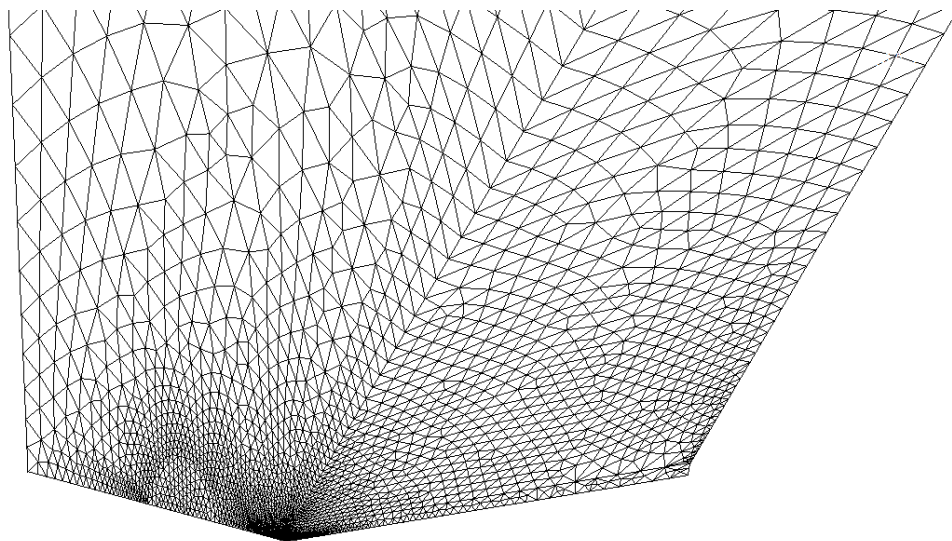
away from the analysed area.

Figure A3. Detail of the mesh on blunt V-notched specimen with radius 0.1 mm

References

[1]   T.T. Wohlers, T. Caffrey, R.I. (R. I. Campbell, Wohlers report 2016 : 3D printing and additive manufacturing state of the industry : annual worldwide progress report, n.d. https://wohlersassociates.com/2016report.htm (accessed September 4, 2017).

[2]   K. V. Wong, A. Hernandez, A Review of Additive Manufacturing, ISRN Mech. Eng. 2012 (2012) 1–10. doi:10.5402/2012/208760.

[3]   D.D. Gu, W. Meiners, K. Wissenbach, R. Poprawe, Laser additive manufacturing of metallic components: materials, processes and mechanisms, Int. Mater. Rev. 57 (2012) 133–164. doi:10.1179/1743280411Y.0000000014.

[4]   B. Vayre, F. Vignat, F. Villeneuve, Metallic additive manufacturing: state-of-the-art review and prospects, Mech. Ind. 13 (2012) 89–96. doi:10.1051/meca/2012003.

[5]   M. Crespo, M.T. Gómez-del Río, J. Rodríguez, Failure of SLS polyamide 12 notched samples at high loading rates, Theor. Appl. Fract. Mech. 92 (2017) 233–239. doi:10.1016/J.TAFMEC.2017.08.008.

[6]   Z. Doubrovski, J.C. Verlinden, J.M.P. Geraedts, Optimal Design for Additive Manufacturing: Opportunities and Challenges, in: Vol. 9 23rd Int. Conf. Des. Theory Methodol. 16th Des. Manuf. Life Cycle Conf., ASME, 2011: pp. 635–646. doi:10.1115/DETC2011-48131.

[7]   A.G.M. Michell, LVIII. *The limits of economy of material in frame-structures*, Philos. Mag. Ser. 6. 8 (1904) 589–597. doi:10.1080/14786440409463229.

[8]   B. Bickel, M. Bächer, M.A. Otaduy, H.R. Lee, H. Pfister, M. Gross, W. Matusik, Design and Fabrication of Materials with Desired Deformation Behavior, (n.d.). https://vcg.seas.harvard.edu/files/pfister/files/mat_fab_sig10.pdf (accessed September 13, 2017).

[9]   D.H. Abdeen, B.R. Palmer, Effect of processing parameters of electron beam melting machine on properties of Ti-6Al-4V parts, Rapid Prototyp. J. 22 (2016) 609–620. doi:10.1108/RPJ-09-2014-0105.

[10]   V.S. Sufiiarov, A.A. Popovich, E. V Borisov, I.A. Polozov, D. V Masaylo, A. V Orlov, The effect of layer thickness at selective laser melting, Procedia Eng. 174 (2017) 126–134. doi:10.1016/j.proeng.2017.01.179.

[11]   H. Gong, K. Rafi, H. Gu, G.D. Janaki Ram, T. Starr, B. Stucker, Influence of defects on mechanical properties of Ti–6Al–4 V components produced by selective laser melting and electron beam melting, Mater. Des. 86 (2015) 545–554. doi:10.1016/J.MATDES.2015.07.147.

[12]   T.M. Mower, M.J. Long, Mechanical behavior of additive manufactured, powder-bed laser-fused materials, Mater. Sci. Eng. A. 651 (2016) 198–213. doi:10.1016/J.MSEA.2015.10.068.

[13]   L.E. Murr, E.V. Esquivel, S.A. Quinones, S.M. Gaytan, M.I. Lopez, E.Y. Martinez, F. Medina, D.H. Hernandez, E. Martinez, J.L. Martinez, S.W. Stafford, D.K. Brown, T. Hoppe, W. Meyers, U. Lindhe, R.B. Wicker, Microstructures and mechanical properties of electron beam-rapid manufactured Ti–6Al–4V biomedical prototypes compared to wrought Ti–6Al–4V, Mater. Charact. 60 (2009) 96–105. doi:10.1016/J.MATCHAR.2008.07.006.

[14]   J. Tong, C.R. Bowen, J. Persson, A. Plummer, Mechanical properties of titanium-based Ti–6Al–4V alloys manufactured by powder bed additive manufacture, Mater. Sci. Technol. 33 (2017) 138–148. doi:10.1080/02670836.2016.1172787.

[15]   X. Zhao, S. Li, M. Zhang, Y. Liu, T.B. Sercombe, S. Wang, Y. Hao, R. Yang, L.E. Murr, Comparison of the microstructures and mechanical properties of Ti–6Al–4V fabricated by selective laser melting and electron beam melting, Mater. Des. 95 (2016) 21–31. doi:10.1016/j.matdes.2015.12.135.

[16]   P. Ferro, M. Peron, S.M.J. Razavi, F. Berto, J. Torgersen, The fatigue behavior of V-notches in presence of residual stresses: Recent developments and future outcomes, Frat. Ed Integrita Strutt. 11 (2017). doi:10.3221/IGF-ESIS.42.20.

[17]   M. Peron, S.M.J. Razavi, F. Berto, J. Torgersen, F. Mutignani, Local strain energy density for the fatigue assessment of hot dip galvanized welded joints: Some recent outcomes, Frat. Ed Integrita Strutt. 11 (2017). doi:10.3221/IGF-ESIS.42.22.

[18]   M. Peron, S.M.J. Razavi, F. Berto, J. Torgersen, L. Marsavina, Local strain energy density for the fracture assessment of polyurethane specimens weakened by notches of different shape, 4232214223 (2017) 214–222. doi:10.3221/IGF-ESIS.42.23.

[19]   M. Peron, S.M.J. Razavi, F. Berto, J. Torgersen, Notch stress intensity factor under mixed mode loadings: an overview of recent advanced methods for rapid calculation, Frat. Ed Integrità Strutt. 42 (2017) 196–204. http://www.gruppofrattura.it/pdf/fig/numero42/206/ (accessed April 12, 2018).

[20]   A. Campagnolo, S.M.J. Razavi, M. Peron, J. Torgersen, F. Berto, Mode II brittle fracture: Recent developments, Frat. Ed Integrita Strutt. 11 (2017). doi:10.3221/IGF-ESIS.42.19.

[21]   S.M.J. Razavi, M. Peron, J. Torgersen, F. Berto, F. Mutignani, Effect of hot dip galvanization on the fatigue strength of steel bolted connections, Frat. Ed Integrita Strutt. 11 (2017). doi:10.3221/IGF-ESIS.41.54.

[22]   M. Peron, S.M.J. Razavi, F. Berto, J. Torgersen, M. Colussi, Fracture assessment of magnetostrictive materials, Frat. Ed Integrita Strutt. 11 (2017). doi:10.3221/IGF-ESIS.42.24.

[23]   S.M.J. Razavi, M. Peron, F. Mutignani, J. Torgersen, F. Berto, A Study on the Fatigue Behavior of Hot Dip Galvanized Steel Connections, Key Eng. Mater. 754 (2017) 241–243. doi:10.4028/www.scientific.net/KEM.754.241.

[24]   S.M.J. Razavi, M. Peron, F. Mutignani, J. Torgersen, F. Berto, Fatigue Strength of Hot-Dip Galvanized Welded Steel Connections, Key Eng. Mater. 754 (2017) 244–247. doi:10.4028/www.scientific.net/KEM.754.244.

[25]   P. Gallo, S.M.J. Razavi, M. Peron, J. Torgersen, F. Berto, Creep behavior of v-notched components, Frat. Ed Integrita Strutt. 11 (2017). doi:10.3221/IGF-ESIS.41.57.

[26]   S.M.J. Razavi, M. Peron, J. Torgersen, F. Berto, Notched graphite under multiaxial loading, Frat. Ed Integrita Strutt. 11 (2017). doi:10.3221/IGF-ESIS.41.53.

[27]   S.M.J. Razavi, M. Peron, J. Torgersen, F. Berto, T. Welo, 40CrMoV13.9 notched specimens under multiaxial fatigue: an overview of recent results, 41322141 (2017) 440–44655. doi:10.3221/IGF-ESIS.41.55.

[28]   L. Maragoni, P.A. Carraro, M. Peron, M. Quaresimin, Fatigue behaviour of glass/epoxy laminates in the presence of voids, Int. J. Fatigue. 95 (2017) 18–28. doi:10.1016/j.ijfatigue.2016.10.004.

[29]   S.-M.-J. Razavi, P. Ferro, F. Berto, Fatigue Assessment of Ti–6Al–4V Circular Notched Specimens Produced by Selective Laser Melting, Metals (Basel). 7 (2017) 291. doi:10.3390/met7080291.

[30] S.M.J. Razavi, P. Ferro, F. Berto, J. Torgersen, Fatigue strength of blunt V-notched specimens produced by selective laser melting of Ti-6Al-4V, Theor. Appl. Fract. Mech. (2017). doi:10.1016/j.tafmec.2017.06.021.

[31] Fatigue behaviour of notched additive manufactured Ti6Al4V with as-built surfaces, Int. J. Fatigue. 101 (2017) 51–60. doi:10.1016/J.IJFATIGUE.2017.04.009.

[32] R. Branco, J.D. Costa, F. Berto, F.V. Antunes, Fatigue life assessment of notched round bars under multiaxial loading based on the total strain energy density approach, Theor. Appl. Fract. Mech. (2017). doi:10.1016/J.TAFMEC.2017.06.003.

[33] F. Chebat, M. Peron, L. Viespoli, T. Welo, F. Berto, Fatigue Strength Assessment of Steel Rollers: On the Reliability of the Strain Energy Density Approach on Real Components, Appl. Sci. 8 (2018) 1015. doi:10.3390/app8071015.

[34] M. Peron, J. Torgersen, F. Berto, M. Peron, J. Torgersen, F. Berto, A Novel Approach for Assessing the Fatigue Behavior of PEEK in a Physiologically Relevant Environment, Mater. 2018, Vol. 11, Page 1923. 11 (2018) 1923. doi:10.3390/MA11101923.

[35] S.M.J. Razavi, M. Peron, J. Torgersen, F. Berto, Static Multiaxial Fracture Behavior of Graphite Components: A Review of Recent Results, Key Eng. Mater. 754 (2017) 35–38. doi:10.4028/www.scientific.net/KEM.754.35.

[36] M. Peron, S. Razavi, J. Torgersen, F. Berto, Fracture Assessment of PEEK under Static Loading by Means of the Local Strain Energy Density, Mater. 2017, Vol. 10, Page 1423. 10 (2017) 1423. doi:10.3390/MA10121423.

[37] Ł. Derpeński, A. Seweryn, F. Berto, Brittle fracture of axisymmetric specimens with notches made of graphite EG0022A, Theor. Appl. Fract. Mech. 89 (2017) 45–51. doi:10.1016/J.TAFMEC.2017.01.007.

[38] M. Peron, J. Torgersen, F. Berto, Rupture Predictions of Notched Ti-6Al-4V Using Local Approaches, Materials (Basel). 11 (2018) 663. doi:10.3390/ma11050663.

[39] X. Lei, C. Li, X. Shi, X. Xu, Y. Wei, Notch strengthening or weakening governed by transition of shear failure to normal mode fracture, Sci. Rep. 5 (2015) 10537. doi:10.1038/srep10537.

[40] R. Qu, P. Zhang, Z. Zhang, Notch Effect of Materials: Strengthening or Weakening?, J. Mater. Sci. Technol. 30 (2014) 599–608. doi:10.1016/J.JMST.2014.04.014.

[41] Z.F. Zhang, J. Eckert, Unified Tensile Fracture Criterion, Phys. Rev. Lett. 94 (2005). https://journals.aps.org/prl/pdf/10.1103/PhysRevLett.94.094301 (accessed April 16, 2018).

[42] Z.F. Zhang, J. Eckert, L. Schultz, Tensile and fatigue fracture mechanisms of a Zr-based bulk metallic glass, J. Mater. Res. 18 (2003) 456–465. doi:10.1557/JMR.2003.0058.

[43] J.G. Milke, J.L. Beuth, N.E. Biery, Notch Strengthening in Titanium Aluminides under Monotonic Loading, (n.d.). https://link.springer.com/content/pdf/10.1007%2FBF02326488.pdf (accessed April 13, 2018).